DOI: 10.1002/fuce.201200237

SrO-Containing Diopside Glass–Ceramic Sealants for Solid Oxide Fuel Cells: Mechanical Reliability and Thermal Shock Resistance

A. A. Reddy[1], D. U. Tulyaganov[1,2], M. J. Pascual[3], V. V. Kharton[1], E. V. Tsipis[1], V. A. Kolotygin[1], J. M. F. Ferreira[1]*

[1] Department of Materials and Ceramics Engineering, University of Aveiro, CICECO, 3810-193 Aveiro, Portugal
[2] Turin Polytechnic University in Tashkent, 17, Niyazova Str., 100095 Tashkent, Uzbekistan
[3] Instituto de Cerámica y Vidrio (CSIC), C/Kelsen 5, Campus de Cantoblanco, 28049 Mdrid, Spain

Received December 27, 2012; accepted June 04, 2013; published online ■■■

Abstract

A series of glasses and glass–ceramics (GCs) aiming at applications as sealants for solid oxide fuel cells (SOFCs) were synthesized by partial substitution of Ca for Sr in the diopside-Ba disilicate composition. X-ray diffraction in conjunction with the Rietveld-RIR technique were employed to quantify the crystalline (diopside and Sr-diopside) and amorphous phases in the glasses sintered/heat treated at 850 °C in humidified 10%H_2–90%N_2 gas mixture for 250 h. Weibull modulus varied in the range 11.6–34.4 implying toward good mechanical reliability of synthesized GCs. Thermal shock resistance of model electrochemical cells made of yttria-stabilized zirconia, gadolinia-doped ceria, and lanthanum gallate based solid electrolytes, hermetically sealed by one diopside-based composition, was evaluated employing quenching from 800 °C in air and water. Suitable thermal expansion coefficient, mechanical reliability, and strong adhesion to stabilized zirconia and metallic interconnects, are all suggesting a good suitability of the sealants for SOFC applications.

Keywords: Coefficient of Thermal Expansion, Electrolyte, Interconnect, Sealing, Solid Oxide Fuel Cells

1 Introduction

Fuel cells, in particular solid oxide fuel cells (SOFCs), are the most efficient technology to convert chemical energy to electricity. Over the next few years SOFCs are expected to enter the market with satisfactory life-time and performance. Among different designs of SOFC, flat plate (planar) SOFCs became the most promising due to simpler design, easier fabrication, improved performance, and high power density relative to the tubular design. However, these electrochemical cells are still limited by the mechanical behavior of hermetic seals and remain a major challenge in advancing this emerging technology [1–3]. Glasses and glass–ceramics (GCs) materials are becoming the most common sealing materials for SOFC and have been shown to operate in fuel cells for more than 1,000 h with no significant degradation [1–3]. A vast amount of literature is available in this area depicting the failure of glass seals during long-term operation under SOFCs operating conditions [1–10]. Glass and GCs typically exhibit better wetting behavior than metallic sealants, are electrical insulators, and their coefficients of thermal expansion (CTEs) can be tailored to match those of the adjacent hermitic SOFC components in the final joint, thereby minimizing thermally induced stresses and making the SOFCs stack more [2, 3]. However, BaO- and/or SrO-containing glasses may form chromate interfacial phases such as $BaCrO_4$ and $SrCrO_4$, which may lead to mechanical failure of the SOFC stacks [3, 4, 6]. A series of glass compositions recently reported [11] revealed thermophysical properties such as CTE and mechanical strength, viscosity high enough to avoid excessive flow at the elevated temperatures and good sintering ability suitable for SOFC sealants. The Sr-0.3 glass, in particular, demonstrated excellent thermal stability along a period of

[*] *Corresponding author, jmf@ua.pt*

1,000 h at 900 °C and bonded well to the Sanergy HT metallic interconnect and 8YSZ ceramic electrolyte without forming any undesirable interfacial layers at the joints of SOFC components and GC.

However, the mechanical reliability of GC seals during long-term operation in humid atmosphere, the establishment of stable sealing interfaces without forming undesirable phases over long periods of time, and a close matching the CTEs of all SOFCs components under real fuel cell operating conditions [1–3] still remain as big challenges. Based on these considerations and on the getting promising properties of the SrO-containing diopside glass compositions [11], a more in deep study was required aiming at evaluating their suitability for applications as sealants for SOFCs. Being a sequel of the earlier reported work [11], the current study is focused on investigating the following relevant aspects: (i) the fracture behavior and reliability of SrO-containing diopside GCs formed in humidified atmosphere at 850 °C for 250 h using the Weibull statistics; and (ii) the thermal shock resistance of the sealant/oxide electrolyte (SOE) pair joints, using various SOE ceramic compositions.

2 Experimental Procedures

All the glasses, containing appropriate amounts of nine oxides listed in the Table 1, were prepared in the frit form by melt quenching technique. High purity powders of SiO_2 (>99.5%), $CaCO_3$ (>99.5%), $MgCO_3$ (BDH chemicals, UK, >99%), $BaCO_3$ (Sigma–Aldrich, 99.9%), Al_2O_3 (Sigma–Aldrich, >98%), La_2O_3, $SrCO_3$ (Sigma–Aldrich, 99.9%), H_3BO_3 (>99.5%), and NiO (Sigma–Aldrich, 99%) were used. The detailed experimental procedure was mentioned in our previous report [11]. Rectangular bars with dimensions of 4 mm × 5 mm × 50 mm were prepared by uniaxial pressing (80 MPa). The shrinkage, density, mechanical strength, and crystalline phase assemblage of GC sealants were evaluated after the prolonged heat treatment at 850 °C for 250 h in humidified 10%H_2–90%N_2 gas mixture atmosphere, using heating and cooling rates of 5 K min^{-1}. The linear shrinkage was calculated from the difference in the dimensions between the green and the sintered bars. Archimedes' method (i.e., immersion in diethyl phthalate) was employed to measure the apparent density of the sintered GC. The mechanical properties were evaluated by measuring the three-point bending strength (Shimadzu Autograph AG 25 TA, Columbia, MD; 0.5 mm min^{-1} displacement) of sintered and rectified parallelepiped GC bars. The mean values and the standard deviations (SD) presented for, shrinkage, density and bending strength have been obtained from at least eight different samples. The mechanical reliability was tested by applying the well-known Weibull statistics to the experimental data [12]. According to Weibull statistics, the increasing probability of failure (F) for a brittle material can be expressed by $F = 1 - \exp(-\sigma/\sigma_0)^m$, where F is the failure probability for an applied stress (σ), σ_0 is a normalizing parameter known as Weibull characteristic strength, and m is the Weibull modulus. Here, the Weibull modulus m is a measure of the degree of strength data dispersion [13].

Table 1 Nominal batch compositions of the glasses in wt.%.

Glass	CaO	MgO	BaO	SrO	Al_2O_3	La_2O_3	SiO_2	B_2O_3	NiO
Sr-0.1	18.36	16.5	1.36	4.24	2.09	6.67	47.79	2.00	1.00
Sr-0.2	15.74	16.17	1.36	8.31	2.04	6.53	46.84	2.00	1.00
Sr-0.3	13.85	15.85	1.36	12.22	2.00	6.40	45.94	2.00	1.00
Sr-0.4	10.81	15.54	1.36	15.98	1.97	6.28	45.07	2.00	1.00

The qualitative and quantitative analysis of crystalline phases in the GCs (crushed to particle size <45 μm) was made by X-ray diffraction (XRD) analysis using a conventional Bragg-Brentano diffractometer (Philips PW 3710, Eindhoven, The Netherlands) with Ni-filtered Cu-K_α radiation. The quantitative phase analysis of GCs was made by combined Rietveld-RIR (reference intensity ratio) method and further details were explained elsewhere [11]. The values of CTE for GCs were obtained from dilatometry measurements carried out on prismatic samples with a cross section of 4 mm × 5 mm (Bahr Thermo Analyze DIL801 L, Hullhorst, Germany; heating rate 5 K min^{-1}).

To investigate the adhesion and chemical interactions of the glasses with SOFC components, wetting experiments between glasses (powder) – solid electrolyte (8 mol.% yttria-stabilized zirconia-YSZ, Tosoh) and glass-interconnect (Crofer22APU and Sanergy HT) were carried out in humidified 10%H_2–90%N_2 gas mixture atmosphere at 850 °C temperature for 250 h at 2 K min^{-1}. Microstructural observations were made on polished surfaces of the sintered glass powder compacts (chemically etched by immersion in 2 vol.% HF solution for a duration of 2 min) and fractured surfaces of GCs after three point bending strength measurements were observed by scanning electron microscopy (SEM; SU-70, Hitachi). Energy dispersive spectroscopy (EDS; Bruker Quantax, Germany) and line profile measurements to study the distribution of elements along the GC-interconnect diffusion couples were done by SEM Zeiss DSM 950 equipped with microanalysis system EDS Tracor Northern Micro Z-II.

The experimental techniques used to evaluate high-temperature oxygen leakages and thermal shock resistance were described elsewhere [14, 15]. In order to evaluate thermal shock stability of the Sr-0.3 sealant in contact with various solid oxide electrolyte (SOE) ceramics, a series of dense electrolyte membranes made of 8 mol.% yttria-stabilized zirconia, $Ce_{0.8}Gd_{0.2}O_{2-\delta}$ (CGO, Rhodia) and $(La_{0.9}Sr_{0.1})_{0.98}Ga_{0.8}Mg_{0.2}O_{3-\delta}$ (LSGM, Praxair) were sealed onto YSZ tubes (Tosoh) at 900 ± 10 °C during 30 min. Gas-tight SOE disks of YSZ, CGO, and LSGM were sintered at 1,600, 1,500, and 1,400 °C, respectively; their density was higher than 95% of theoretical. After sealing of the electrolyte assemblies and one gas-tightness test at room temperature, each cell was heated up to T_{max} = 800 °C, kept at this temperature during 10–15 min, quenched in air, and then checked for gas-tightness again. This procedure was repeated several times. The cells made of YSZ were successfully tested in 15

air-quenching cycles; for LSGM and CGO disks sealed onto YSZ, cracking and resultant physical leakages were observed after 3 and 4 cycles. SEM analysis of the SOE and GC interfaces was carried out using various combinations of the SOE disks, sealed one to another and quenched in air under identical conditions.

3 Results and Discussion

All the glass compositions were prone for easy casting after 2 h of melting at 1,580 °C resulting in homogeneous and transparent glasses. The amorphous nature of the quenched frits was confirmed by XRD analysis shown in Figure 1. Figure 2a presents X-ray diffractograms of the sintered glass powder compacts heat treated at 850 °C for 250 h in humidified 10%H_2–90%N_2 gas mixture atmosphere. Diopside ($CaMgSi_2O_6$) and Sr-diopside crystallized as the primary crystalline phases in the Sr-0.1, Sr-0.2 GCs, and in Sr-0.3 and Sr-0.4 GCs, respectively. Sr-diopside in Sr-0.1 and Sr-0.2, and diopside in Sr-0.3 and Sr-0.4 appeared as secondary crystalline phases. The standard diffraction patterns of diopside ($CaMgSi_2O_6$; ICDD 078-1390) and Sr-diopside ($Ca_{0.8}Sr_{0.2}MgSi_2O_6$; ICDD: 80-0386) are presented for comparison in Figure 2a. Table 2 presents the quantitative analysis of the crystalline phases as obtained from XRD analysis adjoined with Rietveld-RIR technique. Figure 2b shows the measured XRD pattern fits for Sr-0.3 GC, by using the GSAS EXPGUI software. The calculated diagrams are based on crystallographic structure models, which also take into account specific instrument and sample effects. The parameters of this model have been refined simultaneously using least-squares methods in order to obtain the best fit to all measured data. By least-squares refinement, a so-called figure-of-merit function R has been defined, which describes the residual (agreement) between observed and calculated data [16]. It is noteworthy that many different statistical R factors have been proposed for judging the quality of a Rietveld refinement. The R factors show the mean deviation in accordance with the model used in percent. The "profile R-factor", R_P, and "weighted profile R-factor", R_{wp}, for all the refinements are well within the limits of experimental accuracy. The difference plot in Figure 2b does not show any significant misfits. The differences between the main peaks of diopside and Sr-diopside were due to adjustment difficulties based on the crystalline of the phases. Increasing SrO content in the glasses did not show any significant effect on the total fraction (~85%) of crystalline phase except in Sr-0.2 glass where 92% crystallization was achieved. It should be noted that in the samples heat treated at 850 °C for 250 h in humidified 10%H_2–90%N_2 gas mixture atmosphere a glassy phase content significantly higher (except Sr-0.2) compared to the same samples heat treated at 850 °C for 250 h in air [11]. The positive feature of these GCs is their stable phase assemblage with 85% crystallized fraction after 250 h of heat treatment, whereas the SrO-containing glasses reported by Chou et al. [5, 6] underwent a continuous crystallization process along the aging time up to 2,000 h. The non-variable phase assemblage of the investigated glasses ensures their thermal stability and suitability as sealing materials.

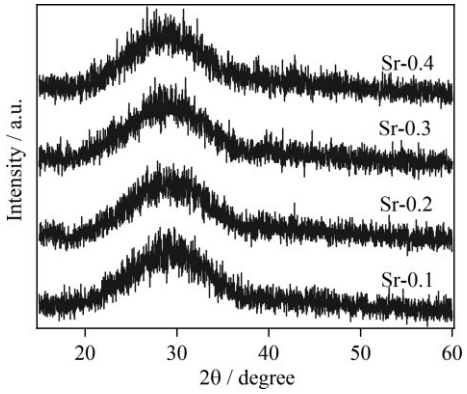

Fig. 1 XRD pattern of as synthesized glasses.

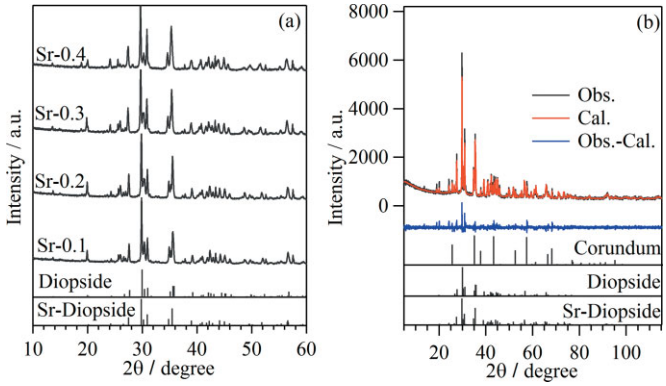

Fig. 2 (a) XRD pattern of GC sintered at 850 °C for 250 h in humidified atmosphere and (b) observed, calculated, and difference curve from the Rietveld refinement of the Sr-0.3 GC heat treated at 850 °C for 250 h in humidified atmosphere.

According to the data summarized in Table 3, well sintered, dense GCs were obtained at 850 °C for 250 h as confirmed by the SEM images of GCs (Figure 3). All the GCs contain very small number of voids in their microstructures. This indicates that a smooth interface between glass and SOFC components can be expected. This was confirmed by interaction studies as discussed later. In general, micro-voids and cracks might be likely due to differential shrinkages and different CTE values between the glass phase and the crystalline phases formed. The shrinkage values varied in the range of 14.7–17.6%, the density increased with increasing SrO content, while bending strength values showed an opposite trend similarly to data obtained in the previous study [11]. Nevertheless, samples heat treated at 850 °C for 250 h in humidified

Table 2 Rietveld RIR (wt.%) results for the GCs heat treated in humidified atmosphere at 850 °C for 250 h.

	Sr-0.1	Sr-0.2	Sr-0.3	Sr-0.4
Diopside	63.5	31.5	25.7	26.7
Sr-diopside	22.2	52.1	60.9	58.3
Glassy phase	14.3	16.4	13.5	15
χ^2	5.44	4.21	2.57	3.53

Table 3 Shrinkage (%), density (g cm^{-3}), bending strength (MPa), Weibull modulus (m), Weibull strength σ_0 (MPa), and CTE (±0.1) × 10^{-6} (K^{-1}) (200–700 °C) data measured for the glass–powder compacts after sintering at 850 °C for 250 h in humidified atmosphere.

Composition	Shrinkage	Density	Bending strength	m	σ_0	CTE
Sr-0.1	14.7 ± 0.4	3.100 ± 0.005	146 ± 11	11.6	146	11.0
Sr-0.2	15.8 ± 0.5	3.160 ± 0.005	139 ± 4	34.4	141	10.0
Sr-0.3	17.3 ± 0.2	3.226 ± 0.003	135 ± 8	17.0	139	10.5
Sr-0.4	17.6 ± 0.3	3.303 ± 0.003	132 ± 8	15.5	136	10.7

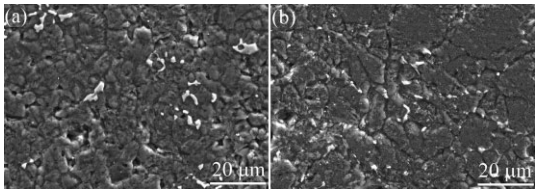

Fig. 3 Microstructure of (a) Sr-0.1 and (b) Sr-0.4 GC heat treated at 850 °C for 250 h in humidified atmosphere.

10%H_2–90%N_2 gas mixture atmosphere demonstrated higher densification level than the same samples heat treated at 900 °C for 250 h in air [11]. This was evident from the observed increments in shrinkage and density values. Under the humidified 10%H_2–90%N_2 gas mixture atmosphere the CTE values of GCs underwent small decreases in comparison to those measured for the samples sintered in air at 900 °C. In general, CTE values for the GCs were reduced with addition of SrO up to Sr-0.2 and increased with the further SrO increments (Table 3). The variation of CTE of the GCs can be explained on the basis of evolution of different crystalline phases and their volume fractions.

As revealed from the XRD analysis and from RIR quantitative analysis, all GCs consist of only two crystalline phases, diopside and Sr-diopside phases. However, establishing an exact correlation between the volume fractions of various phases and the CTE of the GCs is difficult, as the composition of the remaining glass matrix changes with formation of crystalline phases, thereby changing the CTE. A detailed analysis using the standard additive rule will be necessary to account for the contribution of each the phases present in the GC to the thermal expansion of the sealant.

Residual thermal stresses responsible for crack production in glass and GC sealants will always exist in the glass-based seal matrix, even if there is a good match of CTE between the seals and adjacent cell components. During each cycle, the interfaces of the glass and cell components are subjected to thermal stresses between components, typically in the order of 20–150 MPa [17]. Therefore, to overcome these thermal stresses good mechanical reliability for the seals is needed. The two-parameter Weibull analysis was implemented for all the GCs produced at 850 °C. Figure 4a shows that the probability failure function provides a reasonable fit to the data. A large Weibull modulus, called the shape factor m, relates to the uniformity of the distribution of flaws in a brittle material: a high value of m implies a highly uniform distribution of defect sizes and therefore a low level of variability of seal strengths. Conversely, a low value of m implies highly variable flaw sizes and a large spread of measured strengths. The relatively high Weibull modulus, m = 34 for Sr-0.2 and 17 for Sr-0.3, means good mechanical reliability of these sealants. According to Griffith crack theory, when a propagating crack in the compound encounters a crystal with high strength and elastic modulus, the crack direction is deviated by the crystal leading to an increase of the cleavage of the surface. As a result, a higher fracture surface energy is required for crack propagation. The microstructures shown in Figure 5a and b exhibit rough fracture surfaces and thus may be having low crack growth energy. In accordance with the average flexural strength, the Weibull characteristic strength was also reduced in the investigated glasses with increasing SrO contents. The values of Weibull characteristic strength and of average flexural strengths for all the GCs are about 1.5–2.5 times higher than those reported for G-18 glass (51 MPa) [18], GC-9 glass (41–78 MPa) [19], H-sintered bar (55 MPa) [20], and B-sintered bar (91 MPa) [20].

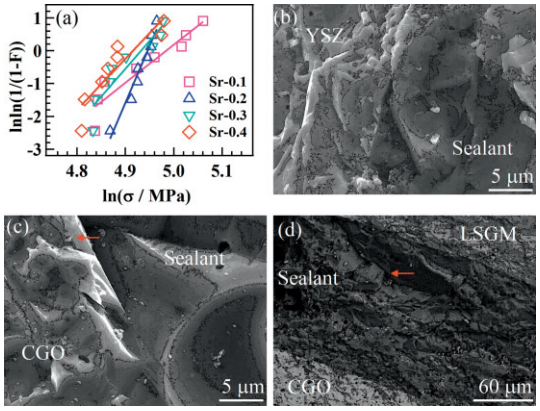

Fig. 4 (a) Weibull distribution of flexural strength for glass–powder compacts annealed at 850 °C for 250 h in humidified atmosphere. (b)–(d) Typical SEM images of the interfaces between Sr-0.3 GC sealant and various solid oxide electrolyte ceramics after 3 air-quenching cycles. The arrows show largest cracks developed at the interfaces.

Figure 6 shows the SEM images of the interfaces between Crofer22APU/GC and Sanergy HT/GC for Sr-0.3 glass, along

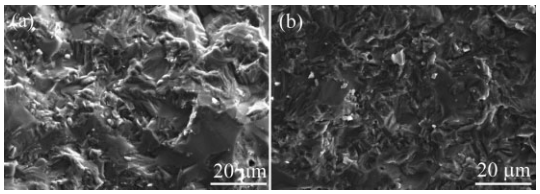

Fig. 5 Microstructure of (a) Sr-0.2 and (b) Sr-0.3 GCs fractured surfaces after the 3 point bending strength measurement.

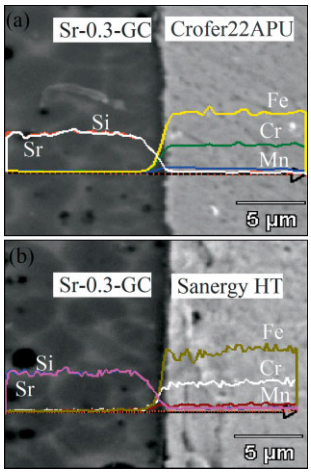

Fig. 6 (a) SEM image and elemental line profile at the interface of Sr-0.3 and Crofer22APU. And (b) SEM image and elemental line profile at the interface of Sr-0.3 and SanergyHT.

with the corresponding EDS elemental mapping of the relevant elements existing at the interface after heat treatment at 850 °C for 250 h in humidified atmosphere. All the GC seals bonded well to the Crofer22APU and Sanergy HT metallic interconnects, no gaps were observed, and the investigated interfaces showed homogeneous microstructures over their entire cross-sections of the joint. The analysis of element mapping (not shown) and elemental profiles confirmed formation of a smooth interface between investigated GC seals and SOFCs Crofer22APU and Sanergy HT metallic plate. Neither spinel nor a chromium oxide layer and any other interfacial reactions were detected at the interfaces by SEM/EDS analyses, within the limits of experimental uncertainty as was observed in case of SrO-containing glasses [4–6, 21]. Further, no negative influence with respect to adhesion and cracking at the interface was observed for the Sr-containing GC sealants. Thus it can be concluded that the Sr-containing diopside glasses could be used within an SOFC stack for hermetic sealing.

The thermal shock resistance tests performed using the Sr-0.3 glass demonstrated the good suitability of this composition for sealing of zirconia-based ceramics. However, further optimization would be required in the case of other electrolytes (CGO or LSGM). For the YSZ electrolyte, a good adhesion and a relatively low CTE mismatch provide sufficient stability during over 15 air-quenching cycles (Table 4) [22–24]. SEM showed no visible cracks at the GC/YSZ interfaces; as an example, Figure 4b presents one SEM image of Sr-0.3/YSZ assembly, which was partly cut and then fractured after 3 air-quenching cycles with T_{max} = 800 °C. For gadolinia-doped ceria, however, the CTE is substantially higher, leading to excessive thermal stresses and failure under identical conditions (Table 4 and Figure 4c). A similar behavior is observed for LSGM electrolyte, although its average CTE is lower than that of doped ceria. Most likely, cracking in the latter case originates from structural transitions of the LSGM perovskite phase; the mechanical properties of LSGM ceramics are also, in general, worse compared to those

Table 4 Average CTEs of solid oxide electrolyte (SOE) ceramics and thermal shock stability of SOE/GC/YSZ assemblies sealed by Sr-0.3 GCs at 900 °C.

Average thermal expansion coefficients				Number of air-quenching cycles
	T °C	$\alpha \times 10^6$ K^{-1}	Reference	
YSZ	25–1,000	10.0	[10]	>15[a)]
CGO	50–1,000	12.5	[11]	4
LSGM	100–1,000	11.1	[12]	3

[a)] The cell remained gastight after 15 air-quenching cycles (T_{max} = 800 °C).

of YSZ and ceria (e.g., see [25] and references cited). Thermal cycling of LSGM/Sr-0.3/CGO assemblies resulted in relatively large cracks (Figure 4d), followed by failure.

The oxygen leakage tests were performed for the model cells comprising a dense YSZ membrane sealed by Sr-0.3 GCs onto tubular support of the same composition. The experiments were carried out in the regime of periodic temperature variations in the range 700–850 °C under large oxygen partial pressure gradient simulating the SOFC operation conditions, 0.21 atm/(10^{-21}–10^{-19}) atm. The results showed that the overall level of oxygen permeation is very low, close to the detection limit. For example, at 800 °C the oxygen fluxes were lower than 5×10^{-13} mol s^{-1}, which is comparable to the experimental error. One should also note that the measured fluxes correspond to the sum of physical leakages originating from microcracks and pores, electrolytic leakage through YSZ due to minor electronic conductivity of stabilized zirconia [25–27], and oxygen transport in the sintered sealant layer separating zirconia ceramics [14, 15]. This combination makes it impossible to estimate area-specific contributions of the components. Consequently, Figure 7a shows the relative variations of the total oxygen flux with time; the corresponding temperature variations are displayed in Figure 7b. The leakage tends to increase with temperature, indicating important roles of possible morphological changes in the sealant at 850 °C and electrolytic permeability increasing with temperature. The significance of the former factor is indicated by the

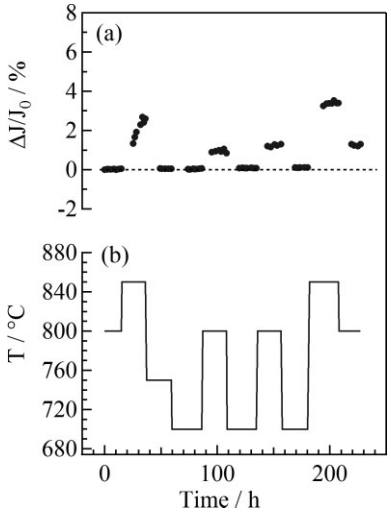

Fig. 7 Time dependence of the relative changes in oxygen leakage flux during thermal cycling of an electrochemical cell with dense YSZ membrane and Sr-0.3 sealant (a), and corresponding temperature variations (b).

fact that no Arrhenius dependence of the oxygen fluxes is observed; on the contrary, heating up to at 850 °C leads to a drastic, essentially irreversible increase of the permeability. Nonetheless, thermal cycling does not induce critical degradation. For example, the resultant increase of the oxygen leakage at 800 °C during 230 h is <2%, i.e., within the limits of experimental uncertainty. This confirms a relatively high quality of the Sr-0.3 GCs as the sealant for high-temperature electrochemical devices with stabilized zirconia electrolytes; the operation temperature should be limited, however, to 750–800 °C.

4 Conclusion

(i) All experimental glass–powder compacts featured higher densification level after sintering at 850 °C for 250 h in humidified 10%H_2–90%N_2 gas mixture atmosphere compared to the samples heat treated at 900 °C for 250 h in air [11].

(ii) Highest mechanical reliability was assigned for compositions Sr-0.2 and Sr-0.3, with Weibull modulus *m* values of 34 and 17, respectively.

(iii) All the GC seals bonded well to Sanergy HT and Crofer22APU metallic interconnects without any interfacial reaction gaps formation.

(iv) The thermal shock resistance tests demonstrated that sealants are suitable for sealing of zirconia-based ceramics. Further optimization will be required for SOFC stacks involving other electrolytes (CGO or LSGM).

5 Acknowledgement

This study was financially supported by the University of Aveiro, CICECO, and FCT, Portugal (SFRH/BD/89915/2012, PTDC/CTM-CER/114209/2009, and PEst-C/CTM/LA0011/2011) and by the Ministry of Education and Science of the Russian Federation (agreement No. 14.825.31.0018).

7 References

[1] E. D. Wachsman, C. A. Marlowe, K. T. Lee, *Energy Environ. Sci.* **2012**, *5*, 5498.
[2] L. Carrette, K. A. Friedrich, U. Stimmimg, *Fuel Cells* **2001**, *1*, 5.
[3] J. W. Fergus, *J. Power Sources* **2005**, *147*, 46.
[4] M. K. Mahapatra, K. Lu, *J. Power Sources* **2010**, *195*, 7129.
[5] Y.-S. Chou, J. W. Stevenson, P. Singh, *J. Power Sources* **2008**, *184*, 238.
[6] Y.-S. Chou, J. W. Stevenson, P. Singh, *J. Electrochem. Soc.* **2007**, *154*, B644.
[7] J. Suffner, U. Dahlmann, *Fuel Cells* DOI: 10.1002/fuce.201200171.
[8] G. Kaur, O. P. Pandey, K. Singh, *Fuel Cells* **2012**, *12*, 739.
[9] I. W. Donald, B. L. Metcalfe, L. A. Gerrard, *J. Am. Ceram. Soc.* **2008**, *91*, 715.
[10] P. K. Ojha, T. K. Chongdar, N. M. Gokhale, A. R. Kulkarni, *J. Power Sources* **2013**, *221*, 28.
[11] A. A. Reddy, D. U. Tulyaganov, M. J. Pascual, V. V. Kharton, V. A. Kolotygin, E. V. Tsipis, J. M. F. Ferreira, *Int. J. Hydrogen Energy* **2013**, *38*, 3073.
[12] D. W. Richerson, *Modern Ceramic Engineering*, 2nd Ed., Marcel Dekker, Inc., New York, USA, **1992**.
[13] W. A. Weibull, S. Stockholm, *J. Appl. Mech.* **1951**, *18*, 293.
[14] M. J. Pascual, V. V. Kharton, E. V. Tsipis, A. A. Yaremchenko, C. Lara, A. Durán, J. R. Frade, *J. Eur. Ceram. Soc.* **2006**, *26*, 3315.
[15] A. Goel, D. U. Tulyaganov, V. V. Kharton, A. A. Yaremchenko, S. Eriksson, J. M. F. Ferreira, *J. Power Sources* **2009**, *189*, 1032.
[16] R. A. Young, *The Rietveld Method. International Union of Crystallography Monographs on Crystallography, in Introduction to Rietveld Method*, Vol. 50 (Ed. R. A. Young), Oxford University Press, Oxford, United Kingdom, **1993**, pp. 1
[17] D. Stolten and B. Edmonts (Eds.), *Fuel Cell Science and Engineering in Materials, Processes, Systems and Technology*, Wiley-VCH, Weinheim, Germany, **2012**.
[18] S. R. Choi, N. P. Bansal, A. Garg, *Mater. Sci. Eng., A* **2007**, *460–461*, 509.
[19] H.-T. Chang, C.-K. Lin, C.-K. Liu, S.-H. Wu, *J. Power Sources* **2011**, *196*, 3583.
[20] J. Malzbender, Y. Zhao, *Fuel Cells* **2012**, *12*, 47.
[21] T. Zhang, R. K. Brow, W. G. Fahrenholtz, S. T. Reis, *J. Power Sources* **2012**, *205*, 301.
[22] M. Mori, T. Abe, H. Itoh, O. Yamomoto, Y. Takeda, T. Kawahara, *Solid State Ionics* **1994**, *74*, 157.
[23] M. Mogensen, T. Lindegaard, U. R. Hansen, G. Mogensen, *J. Electrochem. Soc.* **1994**, *141*, 2122–2128.
[24] A. L. Shaula, V. V. Kharton, F. M. B. Marques, A. V. Kovalevsky, A. P. Viskup, E. N. Naumovich, *J. Solid State Electrochem.* **2006**, *10*, 28.
[25] V. V. Kharton, F. M. B. Marques, A. Atkinson, *Solid State Ionics* **2004**, *174*, 135.
[26] M. Iwase, E. Ichise, M. Takeuchi, T. Yamasaki, *Trans. Jpn. Inst. Met.* **1984**, *25*, 43.
[27] M. Kleitz, M. Levy, J. Fouletier, P. Fabry, *Adv. Ceram.* **1981**, *3*, 337.

